

RESEARCH ARTICLE

Hypoxia Resistance Is an Inherent Phenotype of the Mouse Flexor Digitorum Brevis Skeletal Muscle

Adam J. Amorese^{1,†}, Everett C. Minchew^{1,†}, Michael D. Tarpey¹, Andrew T. Readyoff², Nicholas C. Williamson¹, Cameron A. Schmidt³, Shawna L. McMillin⁴, Emma J. Goldberg¹, Zoe S. Terwilliger¹, Quincy A. Spangenburg¹, Carol A. Witzczak^{5,6,7}, Jeffrey J. Brault^{5,6}, E. Dale Abel⁸, Joseph M. McClung^{1,9,2}, Kelsey H. Fisher-Wellman^{1,9}, Espen E. Spangenburg^{1,9,*}

¹Department of Physiology, Brody School of Medicine, East Carolina University, Greenville, NC 27834, USA,

²East Carolina Diabetes and Obesity Institute, East Carolina University, Greenville, NC 27834, USA,

³Department of Biology, East Carolina University, Greenville, NC 27834, USA, ⁴Department of Kinesiology, East Carolina University, Greenville, NC 27858, USA, ⁵Department of Anatomy, Cell Biology, and Physiology, Indiana University School of Medicine, Indianapolis, IN 46202, USA, ⁶Indiana Center for Musculoskeletal Health, Indianapolis, IN 46202, USA, ⁷Indiana Center for Diabetes and Metabolic Diseases, Indianapolis, IN 46202, USA, ⁸David Geffen School of Medicine, Department of Medicine, University of California, Los Angeles, CA 90095, USA and ⁹Department of Cardiovascular Sciences, Brody School of Medicine, East Carolina University, Greenville, NC 27834, USA

*Address correspondence to E.E.S. (e-mail: spangenburg14@ecu.edu)

[†]These authors contributed equally to this work.

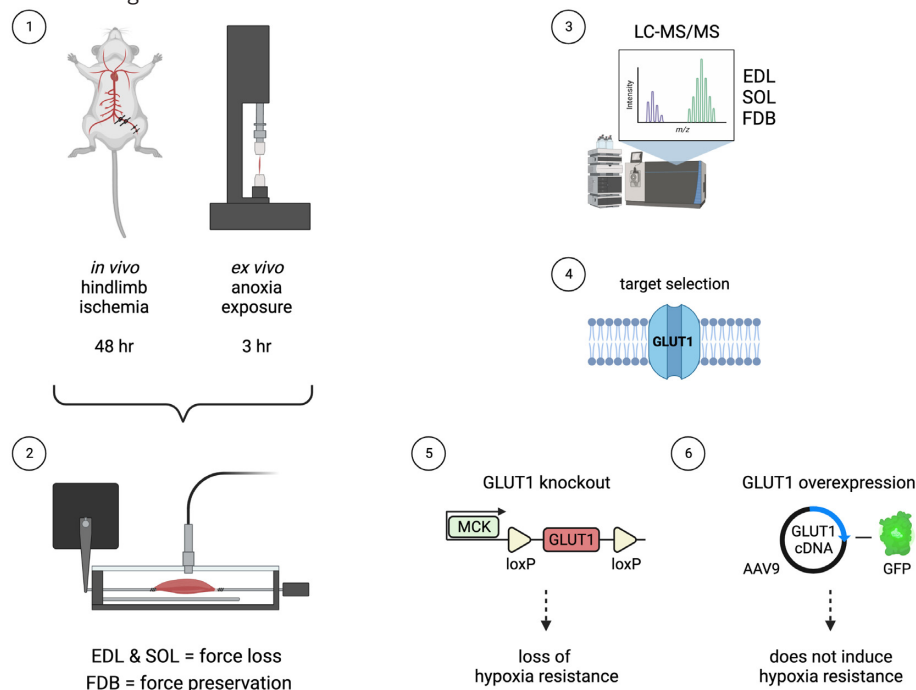
Abstract

The various functions of skeletal muscle (movement, respiration, thermogenesis, etc.) require the presence of oxygen (O₂). Inadequate O₂ bioavailability (ie, hypoxia) is detrimental to muscle function and, in chronic cases, can result in muscle wasting. Current therapeutic interventions have proven largely ineffective to rescue skeletal muscle from hypoxic damage. However, our lab has identified a mammalian skeletal muscle that maintains proper physiological function in an environment depleted of O₂. Using mouse models of *in vivo* hindlimb ischemia and *ex vivo* anoxia exposure, we observed the preservation of force production in the flexor digitorum brevis (FDB), while in contrast the extensor digitorum longus (EDL) and soleus muscles suffered loss of force output. Unlike other muscles, we found that the FDB phenotype is not dependent on mitochondria, which partially explains the hypoxia resistance. Muscle proteomes were interrogated using a discovery-based approach, which identified significantly greater expression of the transmembrane glucose transporter GLUT1 in the FDB as compared to the EDL and soleus. Through loss-and-gain-of-function approaches, we determined that

Submitted: 6 February 2023; Revised: 10 March 2023; Accepted: 13 March 2023

© The Author(s) 2023. Published by Oxford University Press on behalf of American Physiological Society. This is an Open Access article distributed under the terms of the Creative Commons Attribution-NonCommercial License (<https://creativecommons.org/licenses/by-nc/4.0/>), which permits non-commercial re-use, distribution, and reproduction in any medium, provided the original work is properly cited. For commercial re-use, please contact journals.permissions@oup.com

GLUT1 is necessary for the FDB to survive hypoxia, but overexpression of GLUT1 was insufficient to rescue other skeletal muscles from hypoxic damage. Collectively, the data demonstrate that the FDB is uniquely resistant to hypoxic insults. Defining the mechanisms that explain the phenotype may provide insight towards developing approaches for preventing hypoxia-induced tissue damage.



Key words: skeletal muscle; hypoxia; ischemia; resistance; phenotype; mouse

Introduction

Acute or extended bouts of hypoxia or anoxia can induce and/or exacerbate a skeletal muscle myopathy. This myopathy is characterized by the loss of muscle force-producing capacity that contributes directly to overall muscle weakness and potentially leads to reduced functional independence.^{1,2} During lengthy bouts of hypoxia, the inability of skeletal muscle to survive and function becomes a major predictor of mortality and associates with the development of a necrotic pathology.^{3,4} Hypoxia detrimentally affects skeletal muscle in numerous diseases, including various dystrophies, peripheral artery disease, acute traumatic arterial injury/occlusion, and heart failure, as well as elective surgeries such as total knee arthroplasty.^{5–7} Thus, it is critical to define mechanisms and/or approaches that can attenuate hypoxia-induced loss of skeletal muscle function.

A critical gap in developing interventions and/or treatments for hypoxic muscle injury is that the field currently lacks knowledge of the properties reflective of hypoxia resistance. Therefore, the available information is insufficient to reverse engineer a muscle to survive without O₂. This gap is attributable to the fact that the most extensively studied skeletal muscles are sensitive to hypoxia and exhibit damage within minutes of a hypoxic insult.^{8,9} Irrespective of muscle fiber type, skeletal muscle is dependent upon a maintained cellular O₂ tension. O₂ serves as the terminal electron acceptor in the mitochondrial electron transport system (ETS), which is a critical component of meeting the energetic demand of the cell. The extensor digitorum longus (EDL) muscle, for example, is composed predomi-

nantly of fast glycolytic fibers (ie IIb or IIx fibers) and yet requires O₂ to remain viable.¹⁰ Thus, O₂ dependency is a universal phenotype of skeletal muscle.

To induce hypoxia *in vivo*, we employ an animal model in which the femoral artery in the lower limb is transected and ligated, resulting in loss of O₂ tension to distal skeletal muscles. In this model, we have documented a complete loss of force production in the EDL and soleus muscles.¹¹ Current dogma states that tissues located most distal to the site of an arterial occlusion suffer the greatest functional burden and necrotic pathology.¹² However, we surprisingly discovered that the flexor digitorum brevis (FDB)—a muscle located at the bottom aspect of the foot that is among the most distal from the site of artery transection—exhibits a remarkable capacity to maintain function following the same hypoxic insult. Our *in vivo* findings were confirmed using an *ex vivo* approach, during which muscle anoxia exposure significantly impaired function in the EDL and soleus but did not alter the force-producing capacity of the FDB.

Here we reveal that, unlike any other skeletal muscle, the FDB can function properly without O₂ for extended periods of time. Importantly, the FDB provides a unique model system from which the field can gain novel insight toward developing approaches for promoting tissue survival during hypoxia. In this study, we provide a complete characterization of the FDB's ability to resist hypoxic insults and we present data concerning our initial attempts to uncover the underlying mechanism(s). We specifically hypothesized that the FDB relies on glycolytic metabolism to maintain physiological function and meet energetic demands during hypoxia.

Materials and Methods

Animals

The following mice were utilized in the described experiments: 10–12-wk-old male C57BL/6NJ mice ($n = 88$, Jackson Laboratories) and 10–12-wk-old male and female muscle-specific GLUT1 knockout (KO) mice generously provided by Dr. Carol Witczak (Indiana University) and Dr. E. Dale Abel (University of California, Los Angeles). GLUT1 fl/fl mice were bred with muscle creatine kinase Cre recombinase transgenic mice (MCK-Cre⁺; C57BL/6 J strain #005 304; Jackson Laboratories), generating MCK-Cre⁺ (control), GLUT1 fl/fl (WT), or muscle-specific GLUT1 knockout (GLUT1 KO). For these studies, both male and female GLUT1 KO or GLUT1 fl/fl and their wild-type/control littermates ($n = 6–8$ /group) were utilized. Genetic deletion of GLUT1 specifically in the skeletal muscle was confirmed previously by the Witczak lab.¹³ Additionally, our lab confirmed the reduction of GLUT1 mRNA in single FDB muscle fibers via RT-PCR (PowerTrack SYBR Green #A46109, ThermoFisher) in a similar fashion as previously described using primer sequences for GLUT1 (SLC2A1) and HAGH.¹³ No differences were detected in the FDB muscles between the MCK-Cre⁺ (control) and GLUT1 fl/fl (WT) in a preliminary investigation; thus, GLUT1 fl/fl were used as WT mice for the present study.

Mice were housed in a temperature-controlled (22°C) and light-controlled (12/12 h light/dark) facility and allowed *ad libitum* access to food and water. All animal procedures and usage were approved by the Institutional Review Committee at East Carolina University, and animal care complied with the Guide for the Care and Use of Laboratory Animals, Institute of Laboratory Animal Resources, Commission on Life Sciences, National Research Council (Washington: National Academy Press, 1996).

Model of Acute Hindlimb Ischemia

Acute hindlimb ischemia (HLI) was induced in the lower limb as previously described.¹² Briefly, to anesthetize the C57BL/6NJ mice, an intraperitoneal injection of ketamine at 90 mg/kg body weight and xylazine at 10 mg/kg was administered. A small incision was made between the left inguinal fat pad and peritoneum to access the femoral artery, which was then isolated from the femoral vein. Ligatures were placed on the femoral artery in the region distal to the inguinal ligament and the region proximal to the lateral circumflex branch. The femoral artery was subsequently transected at the area between the ligatures. For pain management, mice were administered a subcutaneous injection of buprenorphine at 0.5 mg/kg while recovering. Anesthetized mice were euthanized at various time points following induction of HLI for subsequent analysis.

Histology

Muscle morphology was assessed in control and ischemic muscles via standard hematoxylin and eosin staining methods. Briefly, EDL, soleus, and FDB muscles were frozen in optimal cutting temperature (OCT) media using isopentane submerged in liquid N₂. Transverse cryosections (10 μm) from the muscle mid-belly were cut using a cryostat (Leica 3050S) and adhered to charged glass slides. Sections were air-dried for 10 min prior to standard staining procedures. Following staining, sections were mounted, coverslipped, and imaged using an EVOS FL microscope (Life Technologies) through a 10× objective lens.

Blood Perfusion of the Limb and Paw

Blood perfusion to the lower limb was assessed using laser Doppler perfusion imaging (LDPI), as previously described.¹² Briefly, mice were anesthetized with ketamine/xylazine and placed on a heating pad at 37°C. Using a microshaver, fur was removed from the lower limb, and both plantar paws (4 ms/pixel scan rate) and medial thighs (10 ms/pixel scan rate) were imaged using a LDI2-High Resolution System (830 nm) (Moor Instruments, Moor, Axminster, UK). LDPI was performed prior to HLI surgery, immediately following surgery, and at 24 and 48 h following surgery, prior to sacrifice.

Perfused Vessel Labeling

Quantification of total vessel and perfused vessel content was performed as previously described.¹² Briefly, mice were administered a retro-orbital injection of *Griffonia simplicifolia* isolectin-B₄ Dylight 594 conjugate (Vector Labs, Burlingame, CA) (50 μL of 1 mg/mL) immediately following the induction of HLI. At 6 h post-HLI, EDL and FDB muscles were dissected and frozen in OCT compound (VWR). Transverse cryosections (10 μm) taken from the muscle midbelly were cut using a cryostat (Leica 3050S) and mounted on charged glass slides. Slides were fixed in 1:1 ice-cold methanol/acetone and incubated for 10 min at -20°C. Following 10 min of air drying, sections were rehydrated with ice-cold 1× phosphate buffered saline (PBS) for 5 min. Phosphate buffered saline was subsequently removed, and sections were blocked with PBS-diluted 5% goat serum at room temperature in the dark for 1 h. After removing goat serum, sections were incubated overnight with goat anti-rat CD31 (platelet endothelial cell adhesion molecule) primary antibody (BioRad) (1:100) and anti-dystrophin primary antibody (Abcam ab15277) (1:100) at 4°C. The following day, primary antibodies were removed, and sections were washed three times with ice-cold 1X PBS for 5 min. Secondary antibodies (Alexa Fluor 488 goat anti-rat IgG, Thermo Fisher Scientific A-11006, and Alexa Fluor 647 goat anti-rabbit IgG, Thermo Fisher Scientific A-21244) were subsequently applied to sections (1:250) for incubation at room temperature in the dark for 1 h. Following removal of secondary antibodies and a second round of washing at 3 × 5 min with ice-cold 1X PBS, sections were mounted with Vectashield (Vector Labs) and imaged using an EVOS FL microscope (Life Technologies) through a 20X objective lens. Image quantification was performed using the ImageJ software by measuring the percentage area of Dylight 594 and CD31 positive signal within each image and, representing the data as a ratio of the signals.

Muscle Dissection for Contractile Measurements

EDL, soleus, and FDB muscles were dissected as previously described.¹⁴ Briefly, mice were anesthetized via isoflurane (3%–4%) and muscles dissected, with the mouse euthanized after the tissue was removed. During the dissection of the muscles, 4–0 silk suture was used to tie a double square knot at distal and proximal tendons. Tendons were cut just above the knot, and muscles were submerged in a bath of oxygenated (95% O₂/5% CO₂) Krebs Ringer buffer (KRB) (119 mM NaCl, 5 mM KCl, 5 mM NaHCO₃, 1.25 mM CaCl₂, 1 mM KH₂PO₄, 10 mM HEPES, and 1 mM MgSO₄) at room temperature. To force the muscle to rely on stored substrates, the KRB did not contain any metabolic substrates (eg, glucose). The muscles were dissected from each

animal as quickly as possible and immediately placed in oxygenated KRB. Muscles were affixed to a force transducer apparatus (Aurora Scientific) and equilibrated in the oxygenated KRB bath for 10 min. Following equilibration, optimal muscle length (L_0) was determined by administering maximal twitch stimulations every 30 s and incrementally adjusting muscle L_0 until peak twitch force was achieved.

Muscle Contractile Protocols

Following establishment of L_0 , EDL, soleus, and FDB muscles were subjected to either a force–frequency protocol as previously described,¹⁴ or a 3-h protocol of isometric muscle contraction. We have published a detailed description of the protocol for assessing the contractile function of the FDB, EDL, and soleus.¹⁴ Briefly, silk suture was tied to the proximal and distal tendons of all muscles except for the FDB, where suture is secured to the three medial toe tendons simultaneously. Force–frequency protocols were employed in the oxygenated (95% O_2 /5% CO_2) KRB bath with isometric force measured via sequential administration of 200 ms pulse trains separated by 60 s at 10, 20, 40, 60, 80, 100, and 120 Hz. For the 3-h protocol, isometric force was measured with the administration of 200 ms pulse trains at 100 Hz every 10 min over the course of 3 h. To run the 3-h protocol, the muscles were initially incubated in oxygenated KRB, and resting L_0 was determined as described above. The muscles were either switched to a fresh solution of oxygenated (95% O_2 /5% CO_2) KRB or nitrogenated (95% N_2 /5% CO_2) KRB to simulate anoxia. Using a Clark electrode (Innovative Instruments, Inc), measurable O_2 concentration in the KRB was reduced to undetectable levels ~30 s after the KRB was bubbled with N_2 . Following contractile protocols, L_0 was measured using digital calipers. Muscles were then removed from the force transducer, and tendons were trimmed using micro-scissors. Muscles were blotted dry prior to measuring wet weights. Finally, muscles were flash frozen in liquid N_2 . Specific muscle force (N/cm²) was determined as previously described¹⁵ using predetermined equations.^{14,16}

Pharmacological Inhibition of Mitochondrial Respiration and Glycolysis

To inhibit mitochondrial respiration, muscles were incubated with potassium cyanide (KCN). Cyanide binds the heme-containing subunit of complex IV in the ETS, inhibiting O_2 utilization.¹⁷ Following muscle isolation, determination of L_0 , and measurement of initial normoxic force production, either 2 mM KCN or the equivalent KRB vehicle was added to the bath. Muscles were then subjected to anoxia (95% N_2 /5% CO_2) and completed the 3-h contractile protocol described above. The KCN concentration was determined based on previous work in murine contractile function experiments.¹⁸ We also confirmed that this concentration completely abolished mitochondrial respiration in murine isolated fiber bundles (data not shown).

To inhibit glycolysis, muscles were incubated with bromopyruvate (BrP). Bromopyruvate inhibits the activity of hexokinase and glyceraldehyde 3-phosphate dehydrogenase (GAPDH).¹⁹ Following muscle isolation, determination of L_0 , and measurement of initial normoxic force production, either 500 μ M BrP or the equivalent KRB vehicle was added to the bath. Muscles were then subjected to anoxia (95% N_2 /5% CO_2) and completed the 3-h contractile protocol described above. A concentrations of BrP were tested incrementally between 100 μ M and 1 mM based on

previous studies.^{20,21} 500 μ M was the highest tolerable concentration that did not result in immediate signs of muscle toxicity. Other cell types have been incubated with BrP concentrations as low as 10 μ M²² and as high as 1000 μ M²³ in previous research.

Adenine Nucleotide Measurements

Adenine nucleotides (ATP), adenosine diphosphate (ADP), and adenosine monophosphate (AMP) and inosine monophosphate (IMP) concentrations in EDL, soleus, and FDB muscles were determined using ultra-performance liquid chromatography (UPLC) as previously described.^{24,25} Briefly, muscles were dissected, incubated in oxygenated or nitrogenated KRB for 1 h, and flash frozen in liquid N_2 . Muscles were homogenized using a glass-on-glass homogenizer in cold 3.5% perchloric acid (PCA), and protein was removed via centrifugation. Homogenates were neutralized with 1 M potassium hydroxide (KOH), and adenine nucleotides and IMP concentrations were determined using an Acquity UPLC H class system (Waters, Milford, MA). IMP accumulation is reflective of a mismatch between ATP synthesis and degradation, while a decreased ATP/AMP ratio is indicative of impaired cellular energy status.^{26,27} Concentrations of adenine nucleotides and IMP were normalized to muscle wet weights (mg).

Muscle Proteomics

The proteomes of the EDL, soleus, and FDB muscles were characterized using methods described previously²⁸ with slight modifications. Briefly, muscles from both limbs were dissected from two different male C57BL/6NJ mice and combined to ensure adequate protein yield. Four total muscles were added to 1 mL of urea-based lysis buffer (8 M urea, 50 mM Tris, 40 mM NaCl, 2 mM $MgCl_2$, 10 mM $Na_4P_2O_7$, 50 mM NaF, 50 μ L Halt protease inhibitor cocktail, and 1 PhosSTOP tab), and homogenized on ice using a handheld homogenizer (Kinematica AG). This was repeated four times resulting in four different biological samples per muscle type. Samples were fractionated using the Pierce High pH Reversed-Phase Peptide Fractionation Kit (ThermoFisher Scientific, Cat # 84868), and fractions were frozen on dry ice and lyophilized. Each fraction was resuspended in 0.1% formic acid at a concentration of 0.25 μ g/ μ L following peptide quantification (ThermoFisher Scientific, Cat # 23275). Nano LC–MS/MS analysis was performed as previously described.^{28,29} For data analysis, Proteome Discoverer 2.2 (PDv2.2) and MitoCarta 3.0 were used as previously described²⁸ with significance set at $P < 0.05$. A detailed description of these procedures is provided in the Supplement. All raw data have been deposited in ProteomeXchange (accession # PXD039811) and jPOST (accession # JPST002018).³⁰

Muscle Glycogen Content

Glycogen content was determined by acid hydrolysis and an enzyme-coupled assay to measure D-glucose concentrations, as previously described.¹⁰ Briefly, segments (2–6 mg) of frozen EDL, soleus, and FDB muscles were placed in 125 μ L of 2 M HCl for acid hydrolysis and boiled on a heating block at 95°C for 2 h. Over the course of the 2 h, samples were vortexed every 30 min. Following acid hydrolysis, samples were neutralized with the addition of 125 μ L of 2 N NaOH, and 5 μ L of Tris–HCl pH 7.0 was added to act as a buffer. Samples were vortexed vigorously, and

10 μL of each sample was added to a clear 96-well plate alongside 10 μL of a glucose calibrator (Cima Scientific) and 10 μL of water to act as a blank. A volume of 200 μL of hexokinase reagent (ATP—1.0 mM; glucose-6-phosphate dehydrogenase [G6PDH]—3250 u/L; hexokinase [yeast]—1000 u/L; NAD—1.0 mM) (Cima Scientific) was added to each well and samples incubated at room temperature for 10 min. During this incubation, hexokinase used ATP to catalyze the phosphorylation of glucose to G6P, which is then oxidized with the concomitant reduction of NAD to NADH. Absorbance at 340 nm was measured on a Cytation 5 microtiter plate reader (Biotek, Winooski, VT) to determine the concentration of NADH, which is directly proportional to the concentration of glucose. A linear standard curve (generated by the glucose calibrator) determined the D-glucose concentration in each sample, which was normalized to muscle wet weight (mg).

Muscle Lactate Content

Lactate content was determined using a lactate assay kit (Sigma). Briefly, segments (2–6 mg) of frozen EDL, soleus, and FDB muscles were submerged in 75 μL of 3 M PCA maintained on dry ice. Samples were placed on ice for 15 min to allow the PCA to thaw and penetrate the muscle. Next, samples were incubated at 4°C for 5 min, then refrozen on dry ice. Once the PCA was frozen, 125 μL of 2 M potassium bicarbonate was added to each sample while on dry ice and samples were centrifuged at 4000 $\times g$ for 1 h (4°C). Caps were left open to prevent pressure increases due to CO₂ buildup inside the centrifuge tubes. Following centrifugation, 10 μL of each sample were added to a 96-well plate alongside lactate standards (0, 2, 4, 6, 8, and 10 nmol/well). Lactate assay buffer (Sigma) was added to each well to achieve a final volume of 50 μL . Next, 50 μL of lactate master mix (46 μL lactate assay buffer, 2 μL lactate enzyme mix, and 2 μL lactate probe, Sigma) was added to each well. The plate was then covered for light protection and shaken for 30 min. Absorbance at 570 nm was measured on a Cytation 5 microtiter plate reader (Biotek, Winooski, VT). A linear standard curve (generated by the lactate standards) determined the lactate concentration in each sample, which was normalized to muscle wet weight (mg).

Muscle Ascorbate Content

A colorimetric enzyme-based assay kit (Abcam, ab65656) was used to measure the ascorbate content of the EDL, soleus, and FDB muscles. Briefly, muscles from GLUT1 KO ($n = 16$) and age-matched WT littermates ($n = 14$) were dissected and snap-frozen in liquid N₂. Muscles from two mice were combined to ensure an adequate yield of muscle mass. Combined samples were resuspended in 20 μL of deionized H₂O per mg of tissue and homogenized using a glass-on-glass homogenizer for 10–15 passes. Samples were then centrifuged at 500 $\times g$ for 5 min (4°C) and the supernatant was collected and transferred to a clean microcentrifuge tube. Following completion of the assay procedure, ascorbate content was measured using a 96-well microplate at 593 nm and normalized to total protein content determined by a Pierce BCA Protein Assay Kit (ThermoFisher Scientific), which was carried out in triplicate.

GLUT1 Overexpression

GLUT1 overexpression in the EDL was achieved by injecting GLUT1-GFP cDNA via AAV9 into the anterior compartment of the lower limb of male GLUT1 KO mice (10–12 wk age, $n = 24$ animals). We have previously shown this approach effectively transduces both the TA and EDL muscles.^{31,32} Briefly, animals were anesthetized by isoflurane inhalation (3%–4% or to effect), and after proper surgical depth was obtained, a 29-gauge needle was used to deliver 1.5×10^{11} viral genome particles suspended in 40 μL of sterile 1x PBS to the EDL. Contralateral limbs were injected with an equivalent volume of a PBS vehicle to serve as an internal control. We have previously found that AAV delivery of GFP alone does not affect force production.¹⁴ At 3 wk post-injection, appropriate GLUT1 localization was determined via GFP signal colocalization with dystrophin staining. We repeated the 3-h contractile protocol described above in EDL muscles from GLUT1 KO mice under the following conditions ($n = 8/\text{group}$): GLUT1 alone, GLUT1 + 5 mM glucose, GLUT1 + 50 μM ascorbate (Sigma #A4034), and GLUT1 + 50 μM ascorbate + 50 mU/mL ascorbate oxidase (Sigma #A0157). Glucose, ascorbate, and ascorbate oxidase were added directly to fresh KRB that replaced unsupplemented KRB at the time of the experiments. The glucose concentration was based on circulating concentrations in a lean mouse, and ascorbate concentrations were based on previously described cell culture experiments.³³

Statistical Analysis

All data are presented as mean \pm SEM. Statistical analyses were performed using GraphPad Prism (Version 9.0; DotMatics). One-way or two-way ANOVA with Tukey's multiple comparisons test was used for comparisons of group means when appropriate. Two-tailed t-tests were used when appropriate. For all statistical tests, $P < 0.05$ was considered statistically significant.

Results

Short Term HLI Does Not Cause Functional or Structural Damage in the FDB

Ex vivo isometric force production and muscle histomorphology were assessed in the EDL, soleus, and FDB following 48 h of HLI. Previous work from our lab has demonstrated nearly a complete loss of force-producing capacity in skeletal muscles distal to the ligation site.¹¹ In agreement, the EDL (Figure 1A, $P < 0.00005$) and soleus (Figure 1B, $P < 0.005$) exhibited a significant loss in specific force post-HLI compared to the muscles from the contralateral control limb. In contrast, the FDB lacked any measurable loss in force output despite the same insult (Figure 1C). Histological assessment revealed the presence of severe myopathy in the ischemic EDL and soleus, as demonstrated by fibrotic lesions within the interstitium and altered myofiber morphology (Figure 1D). The FDB, however, did not exhibit typical signatures of ischemia-induced myopathy at the same time point (Figure 1D).

Perfusion to the FDB Is Not Detectable in the HLI Model

Blood flow to the paw as assessed by LDPI in the ischemic limb was reduced immediately after HLI surgery (0 h, Figure 2A) and remained depressed through the 48-h timepoint (Figure

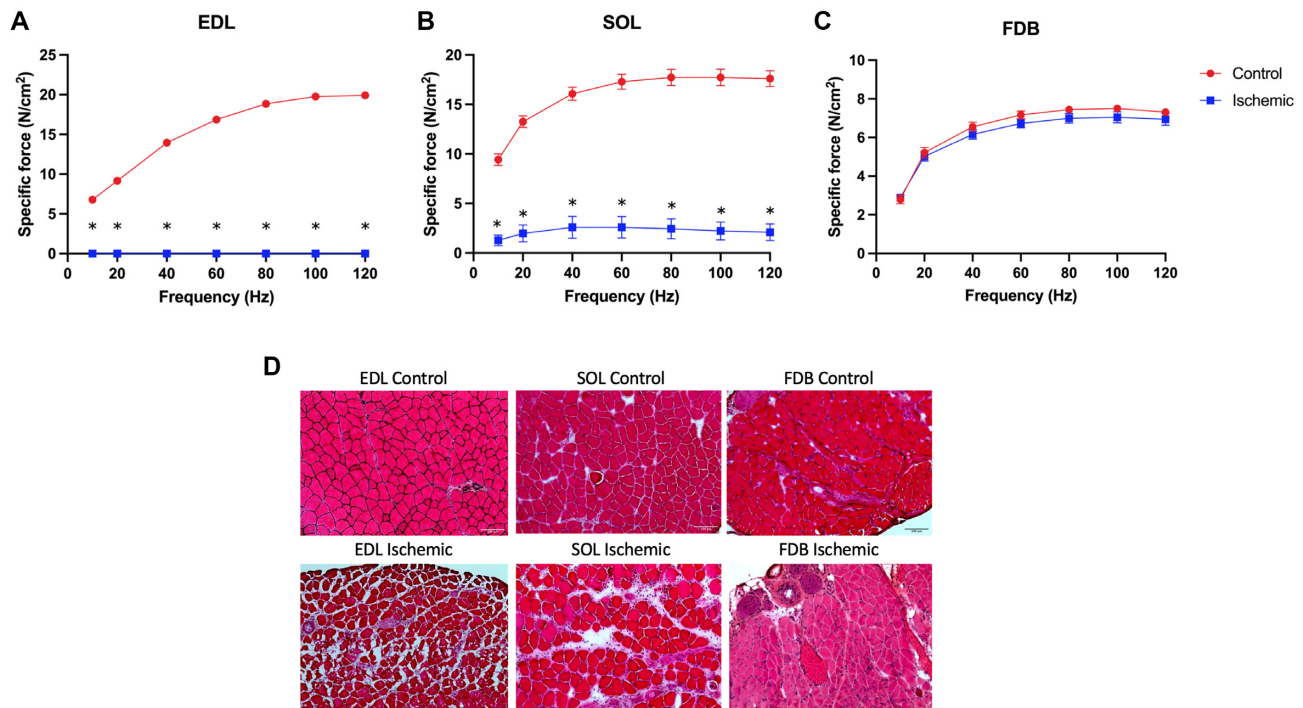


Figure 1. (A–C) *In vivo* HLI leads to functional and structural damage in the EDL and soleus, but not the FDB. Force–frequency curves from control (red) and ischemic (blue) EDL ($P < 0.00005$ compared to contralateral control), soleus ($P < 0.005$ compared to contralateral control), and FDB muscles at 48 h post-HLI. Muscles were stimulated to contract over a range of increasing frequencies, and force output was plotted at each stimulation. (D) Representative cross-sectional images of the EDL, soleus, and FDB stained with hematoxylin and eosin at 48 h post-HLI.

2A–B). The paw, where the FDB is located, exhibited a significant loss in blood flow at all timepoints (Figure 2B). We have previously documented a complete loss of O₂ saturation in skeletal muscles distal to the ligation site following induction of HLI.¹² Individual vessel perfusion at the tissue level was confirmed using GS-IB4 lectin delivery, which labels actively perfused vessels.¹² Hindlimb ischemia surgery eliminated tissue level vessel perfusion in the ischemic EDL and FDB but not within the contralateral control muscles (Figure 2C; orange). Quantification of GS-IB4 signal and normalization of GS-IB4 to the number of CD31⁺ vessels (tissue endothelial cells), demonstrated a consistent loss of perfusion to the ischemic EDL and FDB in the HLI limb (Figure 2D–F, $P < 0.0005$).

The FDB Retains Force Production During *Ex Vivo* Anoxia Exposure

To further assess the FDB in a controlled environment, muscles were surgically removed and placed in either a normoxic (O₂) or anoxic (N₂) Krebs–Ringer Buffer (KRB) within an *ex vivo* tissue bath system. The EDL and soleus exhibited a rapid loss in force output as early as 20 min of anoxia exposure when compared to oxygenated control conditions (Figure 3A–B). The FD⁵⁰ (force drop 50) represents the time at which the muscle loses 50% of its initial normoxic force production and is a proxy of the muscle’s sensitivity to hypoxia. The EDL and soleus muscles reached the FD⁵⁰ at a similar timepoint (66.8 and 61.8 min, respectively) during anoxia (Figure 3D). Furthermore, a near-complete loss of force-producing capacity in these muscles was evident at ~2 h following the onset of anoxia exposure (Figure 3A–B). In contrast, the FDB did not lose force output during the first 2 h of anoxia

and maintained a similar percentage of initial force production between normoxic and anoxic conditions until 160 min of the protocol (Figure 3C).

Nucleotide Concentrations Differ Across Anoxic Skeletal Muscles

Mammalian skeletal muscle requires O₂ to derive chemical energy in the form of ATP. The total amount of ATP in a cell is not a driving factor of function, but rather the concentration of ATP ([ATP]) relative to the concentration of ADP ([ADP]). A lower [ATP]/[ADP] or [ATP]/[AMP] ratio is indicative of energetic stress in the tissue.³⁴ Higher [IMP] reflects energetic stress as well. Minimal changes were detected in [ATP] after anoxia exposure across muscles. However, the anoxic EDL and soleus exhibited significantly lower [ATP]/[ADP] and [ATP]/[AMP] ratios compared to contralateral oxygenated muscles (Table 1, $P < 0.05$). Furthermore, IMP concentrations significantly increased in the EDL and soleus following anoxia exposure (Table 1, $P < 0.05$). Remarkably, no differences in either the [ATP]/[ADP] ratio, the [ATP]/[AMP] ratio, or [IMP] were detected between normoxic and anoxic conditions in the FDB (Table 1).

Unlike Other Peripheral Skeletal Muscles, FDB Function Is Not Dependent Upon Mitochondria

Preserved contractile function of the FDB under anoxic conditions suggests either that the muscle uniquely maintains O₂ tension or that the muscle is not dependent upon the mitochondria to regulate energetic charge. To test this question, we

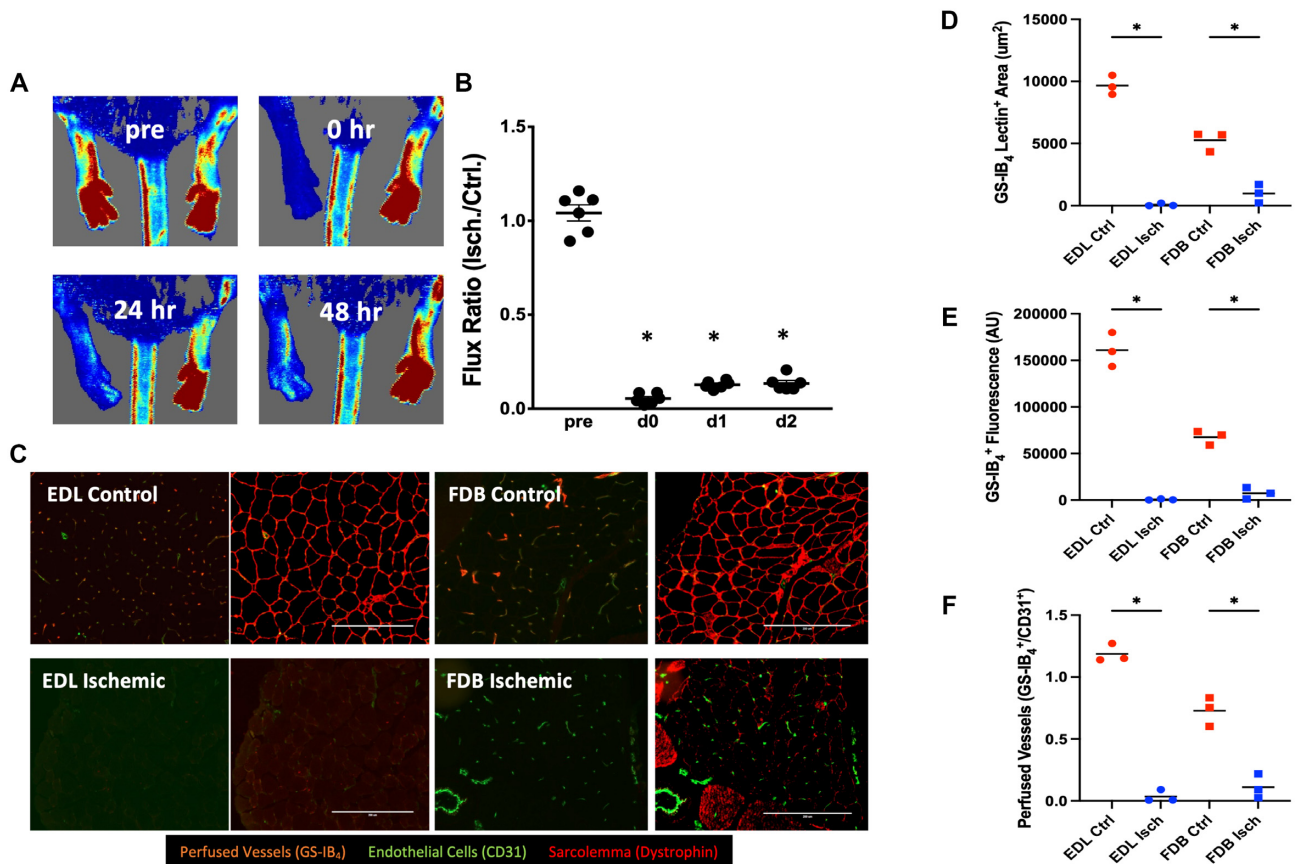


Figure 2. (A–E) *In vivo* HLI causes loss of blood perfusion in skeletal muscles distal to the ligation site. Laser Doppler perfusion imaging (A) and quantification (B) of the paw in the prone position at various time points following induction of HLI. (C) Representative immunofluorescent cross-sectional images of control and ischemic EDL and FDB muscles at 48 h post-HLI. Sections were probed for GS-IB₄ lectin (orange) to label actively perfused vessels, CD31 (green) to label total endothelial cells, and dystrophin (red) to outline the sarcolemma. Loss of blood perfusion to the EDL and FDB was confirmed by measuring the area (D) and fluorescence (E) of GS-IB₄⁺ vessels alongside plotting the signal ratio of GS-IB₄ to CD31⁺ (F). **P* < 0.0005 compared to contralateral control.

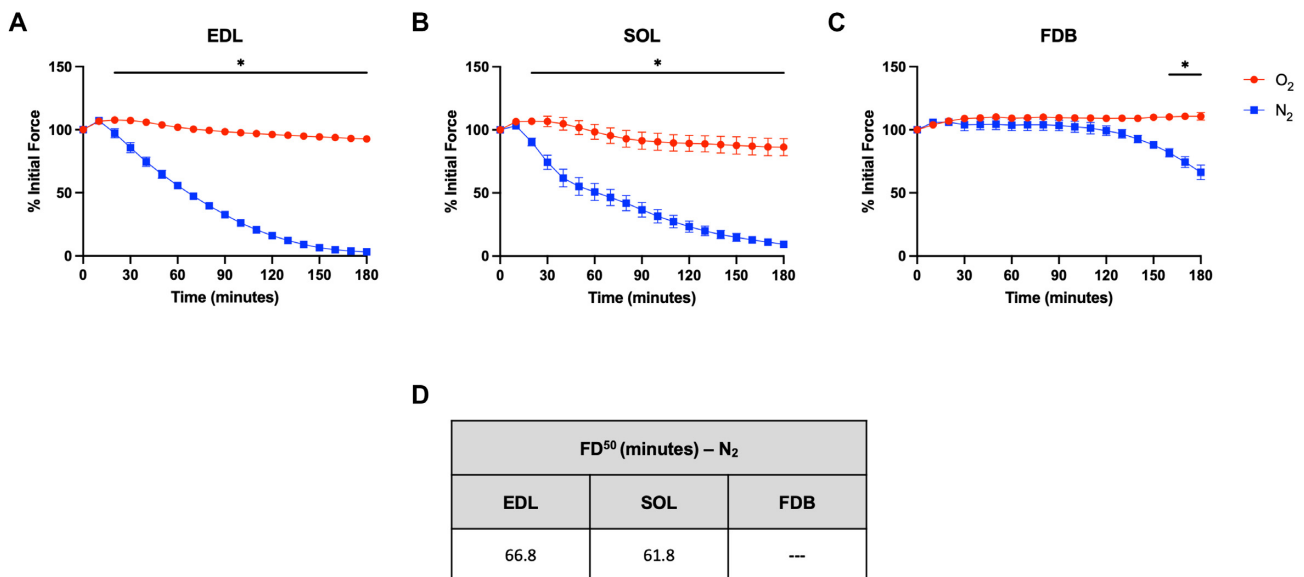


Figure 3. (A–C) *Ex vivo* anoxia exposure leads to force loss in the EDL and soleus, but not the FDB. Initial force output was measured under oxygenated conditions. Muscles were then exposed to 95% O₂/5% CO₂ (normoxia) or 95% N₂/5% CO₂ (anoxia) for 180 min. Muscles were stimulated maximally (100 Hz) every 10 min and force output was measured and plotted as a percentage of the initial normoxic force. FD⁵⁰ represents the time at which force output falls to 50% of the initial normoxic force. **P* < 0.005 compared to the contralateral O₂ condition.

Table 1. Nucleotide ($\mu\text{mol/g}$ wet wt.) in Different Skeletal Muscles Following 1 h of 95% $\text{O}_2/5\%$ CO_2 (Normoxia) or 95% $\text{N}_2/5\%$ CO_2 (Anoxia) Exposure

	ATP			ATP/ADP			ATP/AMP			IMP		
	EDL	SOL	FDB	EDL	SOL	FDB	EDL	SOL	FDB	EDL	SOL	FDB
O_2	6.1 ± 0.2	3.5 ± 0.7	2.1 ± 0.2	5.9 ± 0.3	4.5 ± 0.2	3.2 ± 0.2	505.8 ± 93	121 ± 19	56.7 ± 14.8	0.07 ± 0.02	0.03 ± 0.01	0.02 ± 0.001
N_2	6.1 ± 1	3.0 ± 0.8	2.2 ± 0.2	$4.6 \pm 0.3^*$	$1.8 \pm 0.3^*$	2.8 ± 0.2	$176.3 \pm 2.3^*$	$16.6 \pm 4.6^*$	51.5 ± 12.7	$0.19 \pm 0.04^*$	$0.22 \pm 0.07^*$	0.01 ± 0.003

* $P < 0.05$.

treated muscles with KCN in the *ex vivo* bath to inhibit mitochondrial respiration and simultaneously limit oxygen availability during anoxia exposure. The addition of KCN increased the rate of force loss in the anoxic EDL and soleus as evidenced by a lower FD^{50} compared to anoxia exposure alone (Figure 4D). Significant differences in EDL (Figure 4A, $P < 0.005$) and soleus (Figure 4B, $P < 0.05$) force output between KCN-treated and control conditions were observed as early as 10 min of anoxia exposure. In the FDB, the FD^{50} did not occur until 150.2 min after KCN treatment, whereas the FD^{50} s of KCN-treated EDL and soleus muscles were 37.4 and 23 min, respectively (Figure 4D). Significant differences in FDB force output between conditions were observed after 130 min of anoxia exposure (Figure 4C, $P < 0.05$).

Pharmacological Inhibition of Glycolytic Enzymes Decreases FDB Force Output During Anoxia

Since the FDB's maintenance of energetic charge during anoxia does not appear to rely on the mitochondria, our data would suggest that glycolysis is a major contributor to the function of the FDB. To test this hypothesis, we incubated FDBs with the glycolytic inhibitor BrP, which has been shown to inhibit multiple enzymes in the glycolytic pathway.³⁵ During the 3-h contractile protocol described above, the FD^{50} was reached at 38.7 min in BrP-treated FDBs, which was similar to the EDL (30.2 min) and soleus (23.4 min) under the same conditions (Figure 4H). Significant differences in force output of all three BrP-treated muscles were observed after 10 min of anoxia exposure (Figure 4E–G, $P < 0.05$). In untreated muscles, we found significant differences in glycogen content between the FDB and EDL, but not the soleus (Figure 5A, $P = 0.005$). To determine if anoxia exposure altered glycogen stores, we compared the glycogen content of BrP-treated and vehicle-treated EDL and FDB muscles following anoxia exposure. However, glycogen content did not decrease in either muscle between conditions (Figure 5B–C).

Comprehensive Analysis of the FDB Proteome Compared to the EDL and Soleus Proteome

To further delineate the unique phenotype of the FDB, we compared the proteome of the EDL, soleus, and FDB using TMT-labeled mass spectrometry and identified differential expression patterns of over 2000 proteins across muscles at a significance level of $P < 0.05$ [Figure 6A–B, Supplementary Table S1 (top 75 targets)]. Calculation of the mitochondrial enrichment factor (MEF) found that the mitochondrial protein content detected in the FDB was considerably less than that of the EDL and soleus (MEF; Figure 6C). The MEF represents the number of mitochondrial proteins identified by MitoCarta normalized to the total number of proteins identified by the Proteome Discoverer (>500 different mitochondrial proteins were identified and included in this factor). Heatmap analysis of ETS complex-specific content

across muscles further suggests that mitochondrial respiratory capacity is lower in the FDB than the EDL and soleus (Figure 6D). To characterize mitochondrial function in the FDB, respiration rates were assessed under energetically clamped conditions in permeabilized muscle fiber bundles (PMFB) and in isolated mitochondria from EDL and FDB muscles (Supplementary Figure S1A–B). Across a range of physiologically relevant [ATP]/[ADP] ratios, mitochondrial respiration rates were significantly lower in both PMFB and isolated mitochondria from the FDBs compared to the EDL muscles. These data are consistent with previously published work from our lab.¹⁴ Mitochondrial membrane potential ($\Delta\Psi$) was also significantly lower in mitochondria isolated from the FDB compared to the EDL (Supplementary Figure S1C). Finally, the efficiency of the ETS as assessed by plotting JO_2 vs $\Delta\Psi$ was lower in FDB than EDL mitochondria (Supplementary Figure S1D). The data suggest collectively that relative to mitochondria from the EDL, FDB mitochondria are inefficient and are not critical to overall function. Due to the FDB's relatively low MEF, we hypothesized that glycolytic protein abundance would be greatest in the FDB as compared to the EDL and soleus. However, the number of identified glycolytic proteins normalized to the total number of identified proteins was significantly higher in the EDL than the FDB, although the FDB did contain more glycolytic proteins than the soleus (Figure 6E). These findings were supported by a heatmap analysis of identified glycolytic enzyme content across muscles (Figure 6F).

GLUT1 Is Necessary for the Anoxia-Resistant Phenotype of the FDB

We further refined the proteomics data by examining proteins that were ~2-fold greater and significantly higher in the FDB compared to the EDL and soleus. Considering the deleterious effect of BrP on the force output of the FDB, we focused on targets that might influence glycolytic function. Thus, we selected the transmembrane glucose transporter protein type 1 (GLUT1) as our first target. GLUT1 content in the FDB was 1.9- and 2.1-fold greater than the EDL ($P = 9.4 \times 10^{-5}$, Supplementary Table S1) and soleus ($P = 4.5 \times 10^{-5}$, Supplementary Table S1), respectively. To determine if GLUT1 plays a critical role in the FDB's resistance to anoxia, we employed a skeletal muscle-specific GLUT1 knock-out mouse (GLUT1 KO). Skeletal muscle-specific loss of GLUT1 expression was confirmed via mRNA analysis of single fibers from the FDBs of GLUT1 KO mice (Figure 7A, $P < 0.05$). However, no differences in GLUT1 mRNA were found between whole muscle homogenates of FDBs from GLUT1 KO and WT mice (Figure 7B), indicating that GLUT1 is expressed in non-muscle cells.³⁶ Our data confirm another lab's demonstration of GLUT1 deletion in the skeletal muscle of the GLUT1 KO mice.¹³ To determine whether GLUT1 is necessary for the FDB to maintain force output during anoxia, we repeated the 3-h contractile protocol described above in WT and GLUT1 KO muscles. Deletion of GLUT1 in the FDB resulted in loss of force output, as the FD^{50} in the KO group was reached at 135 min of anoxia exposure,

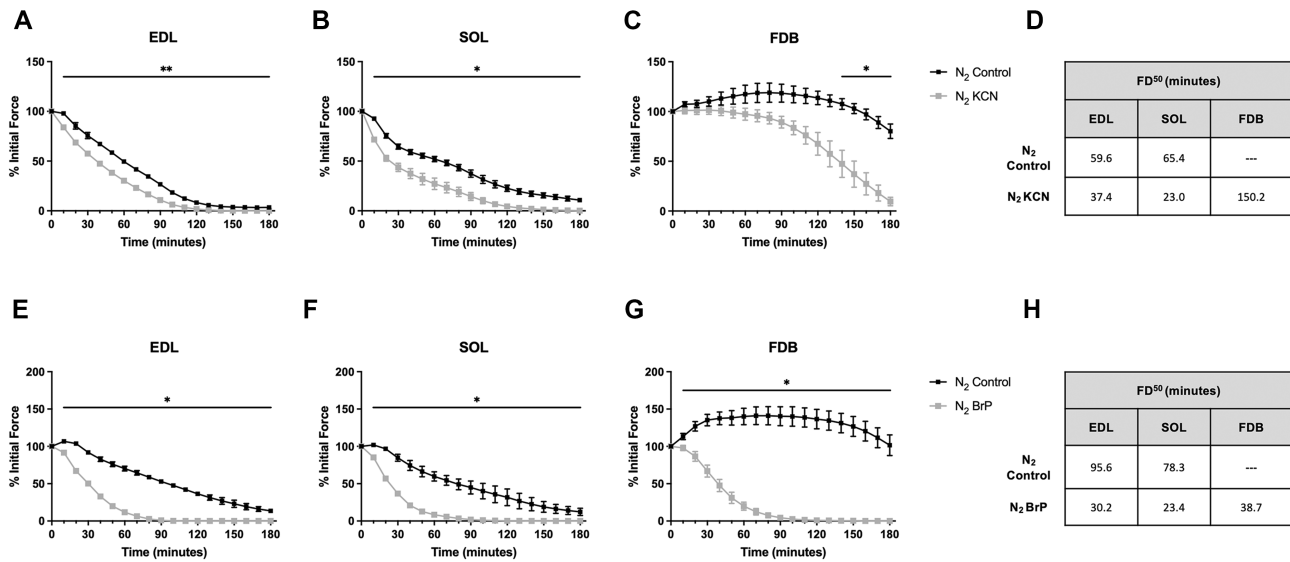


Figure 4. (A–D) Inhibition of mitochondrial respiration during *ex vivo* anoxia exposure accelerates force loss in the EDL and soleus, but not to the same extent in the FDB. Initial force output was measured under oxygenated conditions. Muscles were then exposed to 95% N₂/5% CO₂ (anoxia) for 180 min with or without the addition of KCN to the bath. Muscles were stimulated maximally (100 Hz) every 10 min and force output was measured and plotted as a percentage of the initial normoxic force. * represents a significant difference between the N₂ control and N₂ KCN condition EDL = $P < 0.005$; * soleus = $P < 0.05$; * FDB = $P < 0.05$. (E–H) Inhibition of glycolysis during *ex vivo* anoxia exposure accelerates force loss in the EDL, soleus, and FDB. Initial force output was measured under oxygenated conditions. Muscles were then exposed to 95% N₂/5% CO₂ (anoxia) for 180 min with or without the addition of BrP to the bath. Muscles were stimulated maximally (100 Hz) every 10 min and force output was measured and plotted as a percentage of the initial normoxic force. ** represents a significant difference between the N₂ control and N₂ BrP condition EDL = $P < 0.001$; * soleus = $P < 0.05$; * FDB = $P < 0.001$.

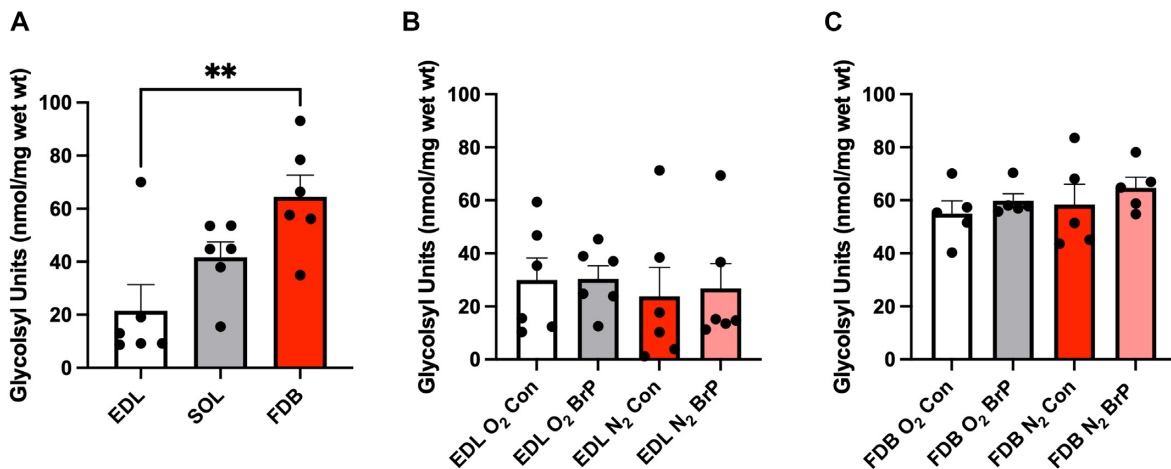


Figure 5. (A) Glycogen content in untreated EDL, soleus, and FDB muscles (** $P = 0.005$). (B) Glycogen content in EDL muscles following the 3-h contractile protocol during normoxia (O₂) or anoxia (N₂) with and without BrP treatment. (C) Glycogen content in FDB muscles following the 3-h contractile protocol during normoxia (O₂) or anoxia (N₂) with and without BrP treatment.

whereas the FD⁵⁰ did not occur in anoxic WT muscles (Figure 7C). Furthermore, FDB force production was significantly different between genotypes after 100 min of anoxia exposure (Figure 7C, $P < 0.05$), whereas no genotype effect was found under oxygenated conditions. Finally, no differences in EDL or soleus force output were found between genotypes compared within conditions (data not shown).

We next compared glycogen and lactate content between WT and GLUT1 KO FDBs during normoxia and anoxia with the hypothesis that the content of both metabolites would be lower in the KO than WT muscles. However, no differences were found between genotypes across conditions (Figure 8A–B). Furthermore, no changes in lactate efflux were found between the EDL and FDB following anoxia exposure (Supplementary Figure

S2). Another substrate imported by GLUT1 in skeletal muscle is the oxidized form of ascorbate—dehydroascorbate.³³ Ascorbate content was significantly greater in the WT FDB compared to WT EDL and soleus muscles (Figure 8C, $P < 0.0001$); however, no differences in ascorbate content were found between WT and GLUT1 KO FDBs (Figure 8C).

GLUT1 Expression Is Insufficient to Prevent Anoxia-Induced Loss of Force Output of the EDL

Following our determination that muscle-specific loss of GLUT1 increased the FDB's susceptibility to anoxia, we assessed whether increasing GLUT1 content in the EDL muscle of GLUT1 KO mice would prevent or attenuate anoxia-induced loss of

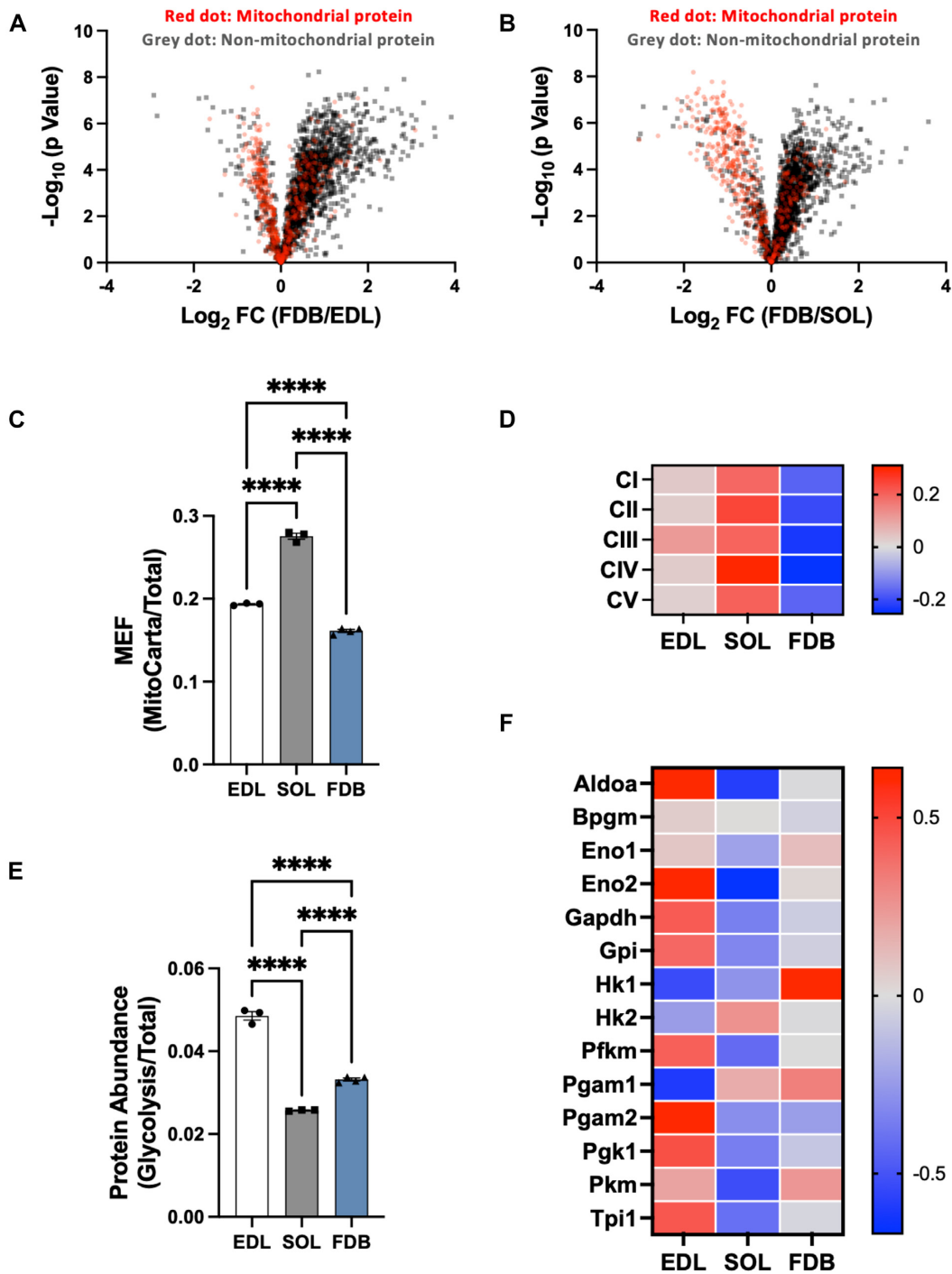


Figure 6. (A–B) Volcano plot of differentially expressed proteins between (A) EDL and FDB muscles and (B) soleus and FDB muscles. Red dots represent mitochondrial proteins, while grey dots represent non-mitochondrial proteins. A leftward position of a dot indicates greater expression in the EDL or soleus, while a rightward position of a dot indicates greater expression in the FDB. An upward position indicates a more significant difference in protein expression between muscles. (C) Quantification of the MEF in the EDL, soleus, and FDB muscles. The MEF represents the number of mitochondrial proteins identified by MitoCarta normalized to the total number of proteins identified by the Proteome Discoverer. (D) Heatmap analysis of mitochondrial ETS complex-specific content in the EDL, soleus, and FDB muscles. Red indicates greater content, while blue indicates lower content. (E) Quantification of identified glycolytic proteins normalized to total proteins identified by the Proteome Discoverer in the EDL, soleus, and FDB muscles. (F) Heatmap analysis of 14 glycolytic enzymes detected in the EDL, soleus, and FDB muscles. Red indicates greater content, while blue indicates lower content. **** $P < 0.0001$.

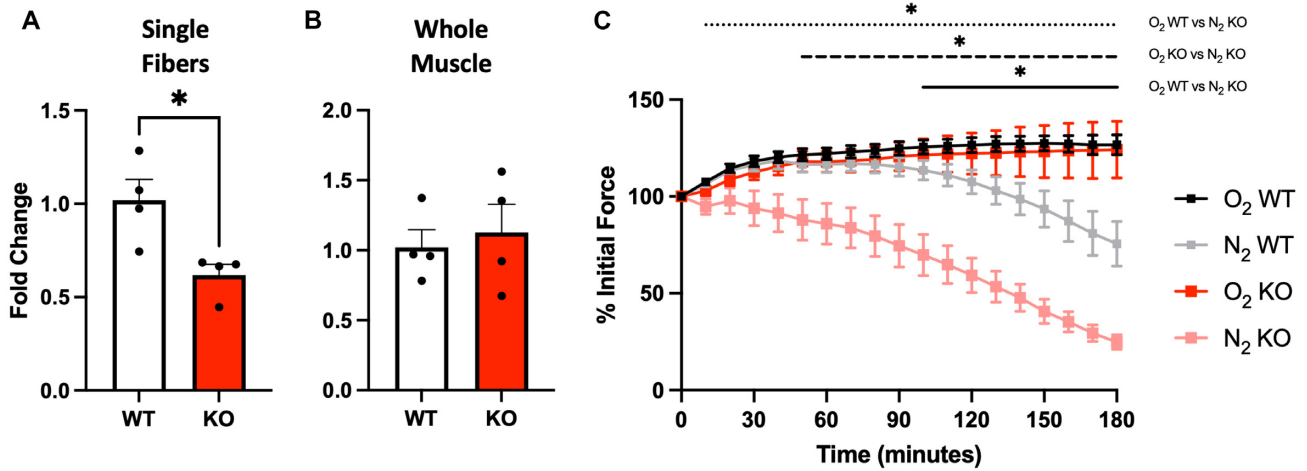


Figure 7. GLUT1 is necessary for the anoxia-resistant FDB phenotype. (A) Validation of decreased GLUT1 mRNA via qRT-PCR analysis in single muscle fibers isolated from FDBs of GLUT1 KO mice as compared to that of WT FDBs ($P < 0.05$ WT vs KO). (B) GLUT1 mRNA quantification via qRT-PCR analysis of whole FDB muscle homogenates from WT and GLUT1 KO mice. (C) Force-time curves of WT and GLUT1 KO FDBs during the 3-h contractile protocol. Initial force output was measured under oxygenated conditions. Muscles were then exposed to 95% O₂/5% CO₂ (normoxia) or 95% N₂/5% CO₂ (anoxia) for 180 min. Muscles were stimulated maximally (100 Hz) every 10 min, and force output was measured and plotted as a percentage of the initial normoxic force. * represents significant difference from N₂ KO; $P < 0.05$.

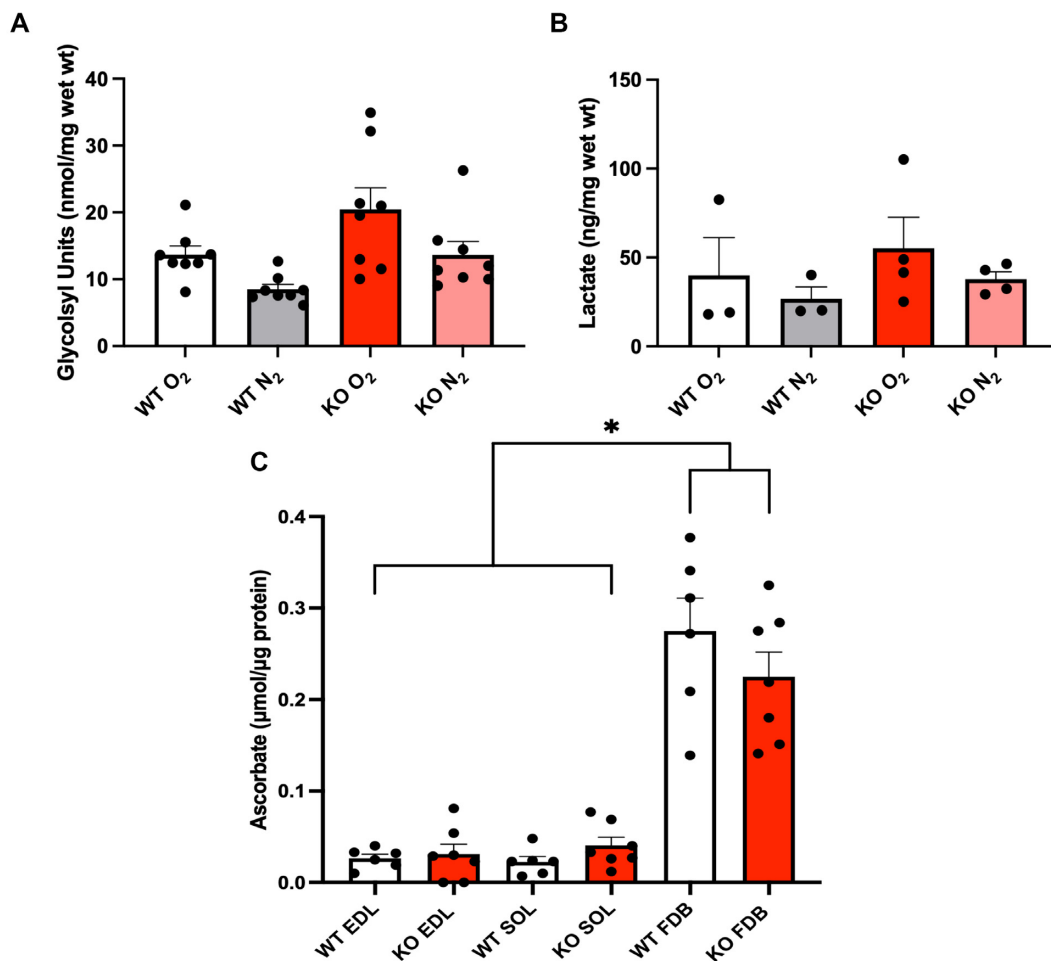


Figure 8. Glycogen (A) and lactate (B) content in FDBs from WT and GLUT1 KO mice following the 3-h contractile protocol during normoxia (O₂) or anoxia (N₂). (C) Ascorbate content in EDL, soleus, and FDB muscles from WT and GLUT1 KO mice. * = main effect of muscle type; $P < 0.0001$.

contractile function in the EDL. GLUT1 overexpression in the EDL was achieved via AAV9-mediated delivery of GLUT1-GFP cDNA. At 3 wk post-injection, GLUT1 was present at the sarcolemma, as evidenced by the signal co-localization of GFP and dystrophin (Figure 9A). Using the gain-of-function approach, the sufficiency of GLUT1 for anoxia resistance in the EDL was assessed under four different conditions: GLUT1 overexpression alone, GLUT1 + glucose, GLUT1 + ascorbate, and GLUT1 + ascorbate + ascorbate oxidase. However, none of the conditions improved the ability of the EDL to retain force output during anoxia (Figure 9B–D; ascorbate oxidase data not shown).

Discussion

It is universally accepted that O₂ is essential to mammalian cell function and survival. Skeletal muscle is among the most metabolically active organ systems, in which O₂ plays a critical role in meeting the high bioenergetic demands of the tissue. Accordingly, hypoxia exposure is a potent insult to muscle function.^{10,37} Hindlimb ischemia surgery results in functional and histomorphological disruption in the EDL and soleus muscles. In contrast, the FDB maintains force production and structural integrity despite the same loss of tissue vessel perfusion and O₂ tension. Consistent with *in vivo* findings, the FDB maintained force production during 3 h of *ex vivo* anoxia exposure, whereas the EDL and soleus muscles experienced significant force loss after only 20 min. Using a discovery-based approach, we compared the proteomes of the EDL, soleus, and FDB. We found that GLUT1 content is higher in the FDB compared to the EDL and soleus, and confirmed that GLUT1 is necessary for the FDB phenotype using a skeletal muscle specific GLUT1 KO mouse. However, AAV-mediated overexpression of GLUT1 was unable to improve anoxia resistance in the EDL muscle. Collectively, our data indicate that the FDB contains a unique phenotype that is not seen more central skeletal muscles. It may be possible to leverage this phenotype to identify mechanisms that confer hypoxia resistance.

Loss of O₂ tension during hypoxia decreases the flux of the mitochondrial ETS and, consequently, decreases the free energy available to perform cellular work due to a lower [ATP]/[ADP] ratio.³⁴ Unlike the EDL and soleus, the FDB is able to preserve cellular energy charge during anoxia exposure, as evidenced by the lack of change in the [ATP]/[ADP] ratio. This ability suggests that bioenergetic regulation within the FDB is unique. Skeletal muscle fiber type analysis on the basis of myosin heavy chain (MHC) isoform prevalence is often associated with the metabolic properties of a muscle. For example, IIX and IIB MHC are often linked with glycolytic metabolism, while I and IIA MHC are linked with oxidative metabolism. The FDB is a mixed muscle comprised predominantly of IIA and IIX myofibers with few I and no IIB myofibers.¹⁴ Based on fiber type composition, one would predict that oxidative metabolism plays an integral role in the FDB. Surprisingly, however, our interrogation of basal mitochondrial function revealed that FDB respiration kinetics and $\Delta\Psi$ are far lower than those of the EDL (a fast glycolytic muscle). Furthermore, the EDL contains more mitochondrial proteins than the FDB, as identified by discovery-based proteomics, suggesting that mitochondrial content is relatively low in the FDB. Supporting the notion that mitochondria do not play a key role in the FDB is the relatively small change in anoxic force production when KCN is added to the *ex vivo* bath. In contrast, the EDL and soleus muscles demonstrated a significant loss in force output when exposed to KCN during anoxia. The

longer time to reach the FD₅₀ in the FDB shows that KCN sensitivity is much lower than that of the EDL and soleus. These data suggest the FDB has adopted a phenotype that does not depend upon the mitochondria to meet the energetic demand of the muscle and further does not reflect the muscle fiber type composition.

Inhibition of glycolysis with BrP decreased force production of all three muscles during anoxia, suggesting that glycolysis is necessary for function across muscles. Importantly, the lack of differences in BrP sensitivity indicates that the FDB does not depend upon glycolysis more than other muscles. Interestingly, the sum of glycolytic proteins identified in the FDB was less than that of the EDL, suggesting that the FDB is not upregulating the capacity to perform glycolysis. Discovery-based proteomic analysis determined that GLUT1 content is significantly higher in the FDB compared to the EDL and soleus. While GLUT4 is the predominant insulin- and exercise-responsive glucose transporter in skeletal muscle, GLUT1 is thought to be responsible for basal glucose uptake.^{38,39} We hypothesized that glycogen content would differ across the three included muscles and found that the FDB contains more glycogen than the EDL but not the soleus muscle. We also measured glycogen content following the 3-h contractile protocol during anoxia to assess whether the FDB would contain less glycogen than the EDL at completion. Neither muscle exhibited a large decrease in glycogen content, which was surprising in light of previous research that demonstrated a significant decrease in skeletal muscle glycogen content following anoxia exposure.¹⁰ A key difference in the study by Schmidt et al.¹⁰ is the greater work performed by the muscles during the contractile protocol as compared to our protocol, thus implying greater energetic demand, and potentially explaining lower glycogen content. Also surprisingly, McMillin et al.¹³ recently demonstrated that neither glucose uptake nor glycogen content is altered in skeletal muscles that lack GLUT1 expression, suggesting a complicated role for GLUT1 in skeletal muscle. Our resulting data provide equivocal evidence that pharmacological inhibition of glycolysis via BrP results in loss of FDB force production during anoxia exposure; however, the muscle does not appear to catabolize greater amounts of glucose. It is possible that BrP treatment affected other mechanisms necessary for force production that are independent of glycolysis. However, the literature largely suggests that BrP inhibits multiple glycolytic enzymes.¹⁹ With that said, we cannot rule out any non-specific effects of BrP on force production.

GLUT1 protein levels in adult rodent hindlimb skeletal muscles have been demonstrated to increase during hypoxia.⁴⁰ Such a response may be indicative of metabolic protection during times of limited energy availability. Our data demonstrate greater GLUT1 protein content in the FDB as compared to the soleus and EDL. Thus, to determine if GLUT1 provides for any portion of the protective phenotype in the FDB, we subjected muscles from WT and skeletal muscle-specific GLUT1 KO mice to the 3-h contractile protocol. FDBs from GLUT1 KO mice exhibited an accelerated loss of force output during anoxia compared to FDBs from WT littermate mice, suggesting that GLUT1 is necessary in part to explain the FDB phenotype. Despite the lack of differences in glycogen content between GLUT1 KO and WT FDBs, we found that the WT FDB contains over 13x greater ascorbate than the WT EDL and soleus. We hypothesized that high levels of ascorbate might attenuate oxidative stress in the FDB during anoxia; however, deletion of GLUT1 did not affect FDB ascorbate content. This suggests that another mechanism is responsible for high ascorbate levels in the FDB. GLUT10, for example, also transports oxidized ascorbate.⁴¹

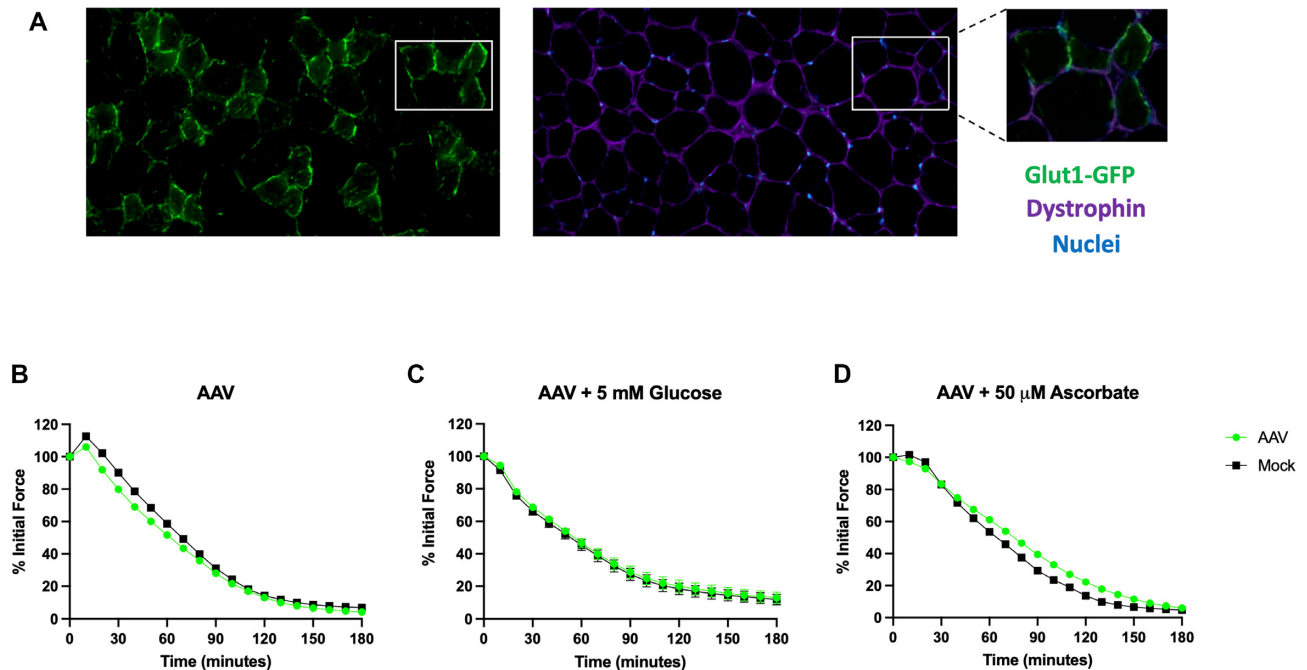


Figure 9. GLUT1 is insufficient to rescue the EDL from anoxic force loss. (A) Representative cross-sectional image of an EDL with GLUT1-GFP overexpression. Sections were probed for nuclei (DAPI, blue) and dystrophin (purple) to confirm successful delivery of the GLUT1-GFP AAV. Note the dystrophin-GFP signal overlay at the sarcolemma. (B–D) Force–time curves of control EDLs (mock, black) and EDLs with GLUT1-GFP overexpression (AAV, green) during the 3-h contractile protocol with anoxia exposure. Three conditions were employed: (B) GLUT1 AAV alone, (C) GLUT1 AAV + glucose, and (D) GLUT1 AAV + ascorbate.

Previous research in smooth muscle cells has shown that GLUT1 overexpression prevents apoptosis during acute hypoxia exposure.⁴² This work is based on a protective effect of increased glucose uptake and glycolytic activity for cardiomyocyte survival under hypoxic conditions.⁴³ To assess if GLUT1 offers protection of other skeletal muscles during anoxia, we overexpressed GLUT1 in the EDL from GLUT1 KO mice using an AAV-mediated delivery. In these experiments, EDLs with GLUT1 were placed in a bath with or without glucose or ascorbate and subjected to the 3-h contractile protocol. To ensure that newly introduced ascorbate was oxidized in the *ex vivo* bath, we also included experiments with added ascorbate oxidase. However, resistance to anoxia-induced loss of EDL force production was not achieved under any condition. Our results indicate that GLUT1 overexpression alone is insufficient to create a protective phenotype in skeletal muscle during anoxia. Furthermore, the FDB phenotype reflects a molecular adaptation that includes increased GLUT1 content but likely requires additional components that are undefined at this time. We speculate that GLUT1 may synergize with other cellular components to protect the FDB during hypoxia.

To our knowledge, this study provides the first evidence of a skeletal muscle that is inherently adapted to maintain its function in the complete absence of O₂. We have thoroughly documented multiple aspects of the FDB phenotype, which provide key evidence to uncovering the muscle's ability to resist hypoxia. Protecting a skeletal muscle from hypoxia is a critical need to improve tissue survival during states of acute hypoxia (eg, altitude) or during various conditions and/or diseases that are associated with muscle atrophy or wasting (eg, PAD, COPD, CHF, and total knee arthroplasty). Identifying the mechanism(s) that confer the FDB phenotype will be instrumental in overcoming these challenges with the goal of leveraging the mechanism(s) in other muscles and potentially in other tissues that are susceptible to

hypoxia. In addition, since no other known murine skeletal muscle can replicate this unique phenotype, the FDB muscle represents a key opportunity to deepen our understanding of skeletal muscle biology. Thus, the physiology of the FDB offers an auspicious opportunity to unlock novel approaches that may promote the viability of mammalian tissue in conditions of limited O₂ bioavailability.

Funding

This work was funded by support from the following grants: National Institutes of Health (NIH) AR078100 (E.E.S.), NIH AR066660 (E.E.S.), NIH HL157659. (J.M.M.), NIH R01AR070200 (J.J.B.), NIH R01DK103562 (C.A.W.), and NIH R21AR081593 (C.A.W.).

Supplementary Material

Supplementary material is available at the APS Function online.

Conflict of Interest

The authors have no conflicts of interest to declare.

Data Availability

The raw data supporting the conclusions of this article will be made available by the authors, without undue reservation.

References

- Berru FN, Gray SE, Thome T, et al. Chronic kidney disease exacerbates ischemic limb myopathy in mice via altered mitochondrial energetics. *Sci Rep* 2019;9(1):1–15.

2. Pipinos II, Judge AR, Selsby JT, et al. Basic science review: the myopathy of peripheral arterial occlusive disease: part 2. oxidative stress, neuropathy, and shift in muscle fiber type. *Vasc Endovascular Surg* 2008;**42**(2):101–112.
3. Chaillou T, Koulmann N, Meunier A, et al. Ambient hypoxia enhances the loss of muscle mass after extensive injury. *Pflugers Arch Euro J Physiol* 2014;**466**(3):587–598.
4. Fitzgerald S, Barlow C, Kampert J, et al. Muscular fitness and all-cause mortality: prospective observations. *J Phys Act Health* 2004;**1**(1):7–18.
5. Mayer C, Franz A, Harmsen JF, et al. Soft-tissue damage during total knee arthroplasty: focus on tourniquet-induced metabolic and ionic muscle impairment. *J Orthop* 2017;**14**(3):347–353.
6. Ryan TE, Yamaguchi DJ, Schmidt CA, et al. Extensive skeletal muscle cell mitochondriopathy distinguishes critical limb ischemia patients from claudicants. *JCI Insight* 2019;**3**(21):e123235.
7. Strassburg S, Springer J, Anker SD. Muscle wasting in cardiac cachexia. *Int J Biochem Cell Biol* 2005;**37**(10):1938–1947.
8. Fredsted A, Mikkelsen UR, Gissel H, Clausen T. Anoxia induces Ca²⁺ influx and loss of cell membrane integrity in rat extensor digitorum longus muscle. *Exp Physiol* 2005;**90**(5):703–714.
9. Shamsadeen NM, Duncan CJ. Effects of anoxia on cellular damage in the incubated mouse diaphragm. *Tissue Cell* 1989;**21**(6):857–861.
10. Schmidt CA, Goldberg EJ, Green TD, et al. Effects of fasting on isolated murine skeletal muscle contractile function during acute hypoxia. *PLoS One* 2020;**15**(4):e0225922.
11. Goldberg EJ, Schmidt CA, Green TD, et al. Temporal association between ischemic muscle perfusion recovery and the restoration of muscle contractile function after hindlimb ischemia. *Front Physiol* 2019;**10**:804.
12. Schmidt CA, Amorese AJ, Ryan TE, et al. Strain-dependent variation in acute ischemic muscle injury. *Am J Pathol* 2018;**188**(5):1246–1262.
13. McMillin SL, Evans PL, Taylor WM, et al. Muscle-specific ablation of glucose transporter 1 (GLUT1) does not impair basal or overload-stimulated skeletal muscle glucose uptake. *Biomolecules* 2022;**12**(12):1734.
14. Tarpey MD, Amorese AJ, Balestrieri NP, et al. Characterization and utilization of the flexor digitorum brevis for assessing skeletal muscle function. *Skelet Muscle* 2018;**8**(1):14.
15. Minchew EC, Williamson NC, Readyoff AT, McClung JM, Spangenburg EE. Isometric skeletal muscle contractile properties in common strains of male laboratory mice. *Front Physiol* 2022;**13**:2046.
16. Brooks SV, Faulkner JA. Contractile properties of skeletal muscles from young, adult and aged mice. *J Physiol* 1988;**404**(1):71–82.
17. Leavesley HB, Li L, Prabhakaran K, Borowitz JL, Isom GE. Interaction of cyanide and nitric oxide with cytochrome c oxidase: implications for acute cyanide toxicity. *Toxicol Sci* 2008;**101**(1):101–111.
18. Zhang SJ, Andersson DC, Sandström ME, Westerblad H, Katz A. Cross bridges account for only 20% of total ATP consumption during submaximal isometric contraction in mouse fast-twitch skeletal muscle. *Am J Physiol Cell Physiol* 2006;**291**(1):C147–C154.
19. Shoshan MC. 3-bromopyruvate: targets and outcomes. *J Bioenerg Biomembr* 2012;**44**(1):7.
20. Park DR. Glycolysis mediated sarcoplasmic reticulum Ca²⁺ signal regulates mitochondria Ca²⁺ during skeletal muscle contraction. *Exerc Sci* 2017;**26**(3):229–237.
21. Jardim-Messeder D, Camacho-Pereira J, Galina A. 3-Bromopyruvate inhibits calcium uptake by sarcoplasmic reticulum vesicles but not SERCA ATP hydrolysis activity. *Int J Biochem Cell Biol* 2012;**44**(5):801–807.
22. Attia YM, EL-Abhar HS, Al Marzabani MM, Shouman SA. Targeting glycolysis by 3-bromopyruvate improves tamoxifen cytotoxicity of breast cancer cell lines. *BMC Cancer* 2015;**15**(1):1–14.
23. Ehrke E, Arend C, Dringen R. 3-bromopyruvate inhibits glycolysis, depletes cellular glutathione, and compromises the viability of cultured primary rat astrocytes. *J Neurosci Res* 2015;**93**(7):1138–1146.
24. Brault JJ, Pizzimenti NM, Dentel JN, Wiseman RW. Selective inhibition of ATPase activity during contraction alters the activation of p38 MAP kinase isoforms in skeletal muscle. *J Cell Biochem* 2013;**114**(6):1445–1455.
25. Davis PR, Miller SG, Verhoeven NA, et al. Increased AMP deaminase activity decreases ATP content and slows protein degradation in cultured skeletal muscle. *Metabolism* 2020;**108**:154257.
26. Baldwin J, Snow RJ, Carey MF, Febbraio MA. Muscle IMP accumulation during fatiguing submaximal exercise in endurance trained and untrained men. *Am J Physiol Regul Integr Comp Physiol* 1999;**277**(1):R295–R300.
27. Hardie DG. Minireview: the AMP-activated protein kinase cascade: the key sensor of cellular energy status. *Endocrinology* 2003;**144**(12):5179–5183.
28. McLaughlin KL, Kew KA, McClung JM, Fisher-Wellman KH. Subcellular proteomics combined with bioenergetic phenotyping reveals protein biomarkers of respiratory insufficiency in the setting of proofreading-deficient mitochondrial polymerase. *Sci Rep* 2020;**10**(1):1–10.
29. Fisher-Wellman KH, Draper JA, Davidson MT, et al. Respiratory phenomics across multiple models of protein hyperacylation in cardiac mitochondria reveals a marginal impact on bioenergetics. *Cell Rep* 2019;**26**(6):1557–1572.
30. Okuda S, Watanabe Y, Moriya Y, et al. jPOSTrepo: an international standard data repository for proteomes. *Nucleic Acids Res* 2017;**45**(D1):D1107–D1111.
31. McClung JM, McCord TJ, Ryan TE, et al. A BAG3 coding variant in mice determines susceptibility to ischemic limb muscle myopathy by directing autophagy. *Circulation* 2017;**136**(3):281–296.
32. Ryan TE, Schmidt CA, Tarpey MD, et al. PFKFB3-mediated glycolysis rescues myopathic outcomes in the ischemic limb. *JCI Insight* 2020;**5**(18):e139628.
33. Eccardt A, Bell T, Mattathil L, Prasad R, Kelly S, Fisher J. Trans-plasma membrane electron transport and ascorbate efflux by skeletal muscle. *Antioxidants* 2017;**6**(4):89.
34. Neuffer PD. The bioenergetics of exercise. *Cold Spring Harb Perspect Med* 2018;**8**(5):a029678.
35. Cardaci S, Desideri E, Ciriolo MR. Targeting aerobic glycolysis: 3-bromopyruvate as a promising anticancer drug. *J Bioenerg Biomembr* 2012;**44**(1):17–29.
36. Wertheimer E, Sasson S, Cerasi E, Ben-Neriah Y. The ubiquitous glucose transporter GLUT-1 belongs to the glucose-regulated protein family of stress-inducible proteins. *Proc Natl Acad Sci* 1991;**88**(6):2525–2529.

37. Godt RE, Nosek TM. Changes of intracellular milieu with fatigue or hypoxia depress contraction of skinned rabbit skeletal and cardiac muscle. *J Physiol* 1989;**412**(1): 155–180.
38. Richter EA, Hargreaves M. Exercise, GLUT4, and skeletal muscle glucose uptake. *Physiol Rev* 2013;**93**(3): 993–1017.
39. Kraegen EW, Sowden JA, Halstead MB, et al. Glucose transporters and in vivo glucose uptake in skeletal and cardiac muscle: fasting, insulin stimulation and immunoisolation studies of GLUT1 and GLUT4. *Biochem J* 1993;**295**(1): 287–293.
40. Xia Y, Warshaw JB, Haddad GG. Effect of chronic hypoxia on glucose transporters in heart and skeletal muscle of immature and adult rats. *Am J Physiol-Regul Integr Comp Physiol* 1997;**273**(5):R1734–R1741.
41. Lee YC, Huang HY, Chang CJ, Cheng CH, Chen YT. Mitochondrial GLUT10 facilitates dehydroascorbic acid import and protects cells against oxidative stress: mechanistic insight into arterial tortuosity syndrome. *Hum Mol Genet* 2010;**19**(19):3721–3733.
42. Lin Z, Weinberg JM, Malhotra R, Merritt SE, Holzman LB, Brosius FC. GLUT-1 reduces hypoxia-induced apoptosis and JNK pathway activation. *Am J Physiol-Endocrinol Metab* 2000;**278**(5):E958–E966.
43. Malhotra R, Brosius FC. Glucose uptake and glycolysis reduce hypoxia-induced apoptosis in cultured neonatal rat cardiac myocytes. *J Biol Chem* 1999;**274**(18):12567–12575.